Brewster angle and reflectivity of optically nonuniform dense plasmas

G. Norman and I. Saitov*

Joint Institute for High Temperatures of RAS, Izhorskaya st. 13, Bld. 2, Moscow 125412, Russia

(Received 22 March 2016; revised manuscript received 22 May 2016; published 6 October 2016)

We provide theoretical analysis of the reflectance of shock-compressed plasmas and warm dense matter for normal incidence of laser radiation as well as for the dependence of s- and p-polarized reflectivity on the incidence angle. The self-consistent approach for the calculation of the optical and electronic properties of warm dense matter and nonideal plasmas developed in our previous works is extended for the description of normal and polarized reflectivity from the broadened optically nonuniform medium. Two methods are applied for the calculation of the reflectivity from spatially broadened optically nonuniform medium. The first one is based on the solution of the Helmholtz equation for the amplitudes of the electromagnetic field. Another one is based on Drude theory of reflection. It allows us to calculate the ratio of the s- and p-polarized reflectivity if dependence of the dielectric function on distance is known. For the case of the polarized reflectivity, the particular attention is concentrated on the Brewster angle. The calculation results for the dielectric function, obtained within the framework of the density-functional theory with the longitudinal expression for the dielectric tensor, are applied for the calculation of the reflectivity. Comparison with the experimental data for shock-compressed xenon is performed.

DOI: 10.1103/PhysRevE.94.043202

I. INTRODUCTION

Measurements and theoretical analysis of optical properties are conventional methods of phase diagram investigations for various substances [1–10], particularly in shock-wave experiments, where the number of the parameters measured is restricted. However, there is a problem when establishing a one-to-one correspondence between optical and electronic properties.

Particular attention is paid to the reflectance of shock-compressed xenon, which is measured in the unique experiments of Mintsev and Zaporoghets [11–14]. There have been many theoretical attempts do describe these experimental data. Taking into account the static effective collisional frequency within the framework of the Drude model [15] does not give a satisfactory explanation of the results obtained. The more accurate expressions for the dynamic effective collisional frequency in the Born approximation [15] do not improve agreement with the experiment. Other attempts to explain experimental results within the framework of the Drude model are associated with an artificial broadening of the wavefront [13–18]. Despite a certain improvement of the agreement with the experiment, this approach does not allow us to establish one-to-one correspondence between the reflectance values and the free charge concentration. Moreover, the agreement with the experiment for normal incidence of laser radiation is reached if the shock front width is 800 nm, which is much higher than the initial theoretical estimation 100 nm [11] (the estimation is based on the evaluation of the xenon ionization rate). The value of the width 220 nm gives satisfactory agreement of theoretical results with the experiment for the dependence of polarized reflectivity on incident angle [14]. However, this value of the width makes the agreement with experiment for the normal reflectance worse.

The approach is suggested for the self-consistent description of optical and electronic properties of nonideal plasmas and warm dense matter [19–23]. It gives a satisfactory description of experiments on normal reflectance of xenon plasmas [19]. The approach is applied for the description of electronic properties of warm dense hydrogen and selenium in the region of the plasma and liquid-liquid phase transitions [22].

In this work, the approach [19–23] is extended to include a description of the normal and polarized reflectance from the broadened shock-wave front. In Sec. II, the method of calculation of the dielectric function and reflectivity within the framework of the density-functional theory (DFT) is briefly discussed. The case of reflection from the ideal shock-wave front is considered. The idea of the self-consistent approach for description of optical and electronic properties of warm dense matter and nonideal plasmas is briefly described. The methods of calculation of normal reflectivity from the nonuniform density profile and comparison with the experimental data [11–13] for xenon plasma are considered in Sec. III. Reflectivity of s- and p-polarized components of the laser radiation from the sharp shock-wave front is discussed in Sec. IV. The calculation method for the polarized reflectivity from the nonuniform shock front profile and comparison with the experimental data [14] is considered in Sec. V. Experimental results for the dependence of s- and p-polarized reflectivity on incident angle [14] are used to investigate the influence of the optical nonuniformity on the optical properties of xenon plasmas. Conclusions are presented in Sec. VI.

II. SELF-CONSISTENT CALCULATION METHOD

The dielectric function (DF) is a complex function and can be expressed as

$$\varepsilon = \varepsilon^{(1)} + i\varepsilon^{(2)}. \tag{1}$$

We consider the interaction of the electromagnetic (transverse) radiation with matter and the response function is the transverse DF. The dependence on frequency ω of the

*saitovilnur@gmail.com

imaginary part of the transverse DF is defined by the following expression in the long-wavelength limit [24]:

$$\varepsilon_T^{(2)}(\omega,\mathbf{R_I}) = (4\pi^2 e^2/3\omega^2\Omega) \lim_{|\mathbf{q}|\to 0} \sum_{n,n',\alpha,\mathbf{k}} 2w_{\mathbf{k}} \times [f(T,E_{n,\mathbf{k}}) - f(T,E_{n',\mathbf{k}+\mathbf{q}})] \cdot |\langle\psi_{n'\mathbf{k}}|\hat{\mathbf{v}}_\alpha|\psi_{n\mathbf{k}}\rangle|^2 \times \delta(E_{n',\mathbf{k}+\mathbf{q}} - E_{n\mathbf{k}} - \hbar\omega), \quad (2)$$

at a given ion configuration $\mathbf{R_I}$ and temperature T, where e is the elementary charge, Ω is a system volume, $\mathbf{q}$ is a wave vector of the incident radiation, and $\hbar$ is the Plank constant. The summation is carried out over all electron states n, n'. The summation over index α multiplied by $1/3$ stands for the averaging over three spatial coordinates. The summation is also carried out over all $\mathbf{k}$ points in the Brillouin zone, taking into account the weights $w_{\mathbf{k}}$ of the $\mathbf{k}$ points. The factor 2 before the weights allows for the electron spin degeneracy. $f(T,E_{n,\mathbf{k}})$ is the Fermi-Dirac distribution function. $E_{n,\mathbf{k}}$ is an eigenvalue (an energy level) corresponding to the wave function $\psi_{n,\mathbf{k}}$, which is a solution of the Kohn-Sham equation. We find this solution as a sum of plane waves and therefore it can be represented by means of the Bloch function $\psi_{n,\mathbf{k}} = e^{i\mathbf{kr}} \cdot u_{n,\mathbf{k}}$, where $u_{n,\mathbf{k}}$ is a cell periodic part. $\hat{\mathbf{v}}$ is the velocity operator.

For local potentials $V(\mathbf{r})$, the expression for velocity operator is equivalent to the momentum operator $\mathbf{p}$: $\hat{\mathbf{v}} = \mathbf{p}/m$, where m is the electron mass. Substitution of this result in (2) gives the Kubo-Greenwood formula [25,26]. For the nonlocal potentials $V(\mathbf{r},\mathbf{r}')$, the additional term arises in the expression for the velocity operator $\hat{\mathbf{v}}$:

$$\hat{\mathbf{v}} = \mathbf{p}/m + (i/\hbar)[V(\mathbf{r},\mathbf{r}'),\mathbf{r}], \quad (3)$$

since the operators of the potential $V(\mathbf{r},\mathbf{r}')$ and distance $\mathbf{r}$ do not commute. It means that the substitution of the wave functions obtained for a Hamiltonian with nonlocal potential into the Kubo-Greenwood formula gives incorrect results. However, the Kubo-Greenwood formula can be used with corrections, which take into account the nonlocality of a projector augmented wave (PAW) potential [3,27–30].

The longitudinal and transverse DF are equal to each other in the long-wavelength limit. In this limit, the velocity operator can be expressed as [31]

$$\hat{\mathbf{v}} = \lim_{|\mathbf{q}|\to 0} \{[\mathbf{p}^2/2m + V(\mathbf{r},\mathbf{r}')], \exp(i\mathbf{qr})\}/\hbar|\mathbf{q}|. \quad (4)$$

The substitution of (4) into (2) gives the expression for the imaginary part of the longitudinal DF [32–34]:

$$\varepsilon_L^{(2)}(\omega,\mathbf{R_I}) = (4\pi^2 e^2/3\Omega) \lim_{|\mathbf{q}|\to 0} \frac{1}{|\mathbf{q}|^2} \sum_{n,n',\alpha,\mathbf{k}} 2w_{\mathbf{k}} \times [f(T,E_{n,\mathbf{k}}) - f(T,E_{n',\mathbf{k}+\mathbf{q}})] |\langle u_{n',\mathbf{k}+\mathbf{e}_\alpha q} \mid u_{n,\mathbf{k}}\rangle|^2 \times \delta(E_{n',\mathbf{k}+\mathbf{q}} - E_{n,\mathbf{k}} - \hbar\omega), \quad (5)$$

where the unit vector $\mathbf{e}_\alpha$ determines the direction of the Cartesian axis corresponding to the coordinate α. Since we use the transformation of the velocity operator (4) for the derivation of (5), the longitudinal expression has no disadvantages, which the Kubo-Greenwood formula has. The formula (5) can be used for any electron-ion potentials.

The eigenvalues and the wave functions are calculated within the framework of the Kohn-Sham DFT approach. Vienna Ab initio Simulation Package (VASP) [35–38] plane-wave code is used in this work for DFT modeling.

It is shown in Refs. [24,39] that the longitudinal expression (5) gives a more correct result in comparison with the widely used Kubo-Greenwood formula within the framework of the PAW approach. The correctness of the expression (5) is confirmed in Refs. [19,40,41], where it is shown that using (5) provides a better explanation of the experimental dependence [11,12,18] of the shocked xenon reflectivity for normal incidence on density in comparison with the Kubo-Greenwood formalism.

The real part of the DF is obtained by the Kramers-Kronig transformation,

$$\varepsilon^{(1)}(\omega,\mathbf{R_I}) = 1 + \frac{2}{\pi} P \int_0^\infty d\omega' \frac{\omega' \varepsilon^{(2)}(\omega',\mathbf{R_I})}{(\omega')^2 - (\omega + i\eta)^2}, \quad (6)$$

where P denotes the principle value (in the limit $\eta \to 0$). It should be noted that expressions (2) and (5) for the DF are obtained for the limit of zero effective collisional frequency ($\eta \to 0$) and are applicable for frequencies $\omega \gg \eta$. However, in nonideal plasmas, the frequency of collisions has finite value. The estimation of the influence of the collisions in plasmas to the optical properties is discussed in Refs. [10,15–17,42,43]. This problem requires a separate, more detailed consideration, which is out of scope of the present work.

The scheme of the approach, which was developed for the calculation of the optical and electronic properties of the dense plasma and warm dense matter (WDM), is shown in Fig. 1.

The theoretical core of the approach is given in two red rectangles. The central red rectangle includes the set of

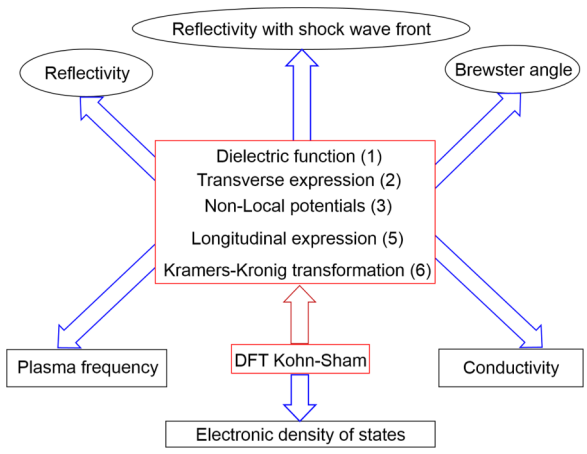

FIG. 1. Scheme of the self-consistent approach for the calculation of optical and electronic properties of warm dense matter and nonideal plasmas. The basis of the self-consistent approach for the calculation of the optical and electronic properties of warm dense matter and nonideal plasmas within the framework of the DFT (two central rectangles) and its applications for the case of the sharp shock front with zero width and the normal incidence of the radiation are represented in Ref. [19]. In the given work, the extension of the approach for the case of normal and polarized reflectivity from the broadened optically nonuniform shock-wave front (upper central and upper right parts of the figure) are considered.

the expressions discussed above. The key expression of the approach is presented by (5), which determines the imaginary part of the complex DF (1). The lower red rectangle indicates the density-functional theory approach, which provides wave functions and energy levels included in expression (5). The core of the method is surrounded by the possible applications, which can be divided into two parts: electronic properties (in the black rectangles) and optical properties (in the black ellipses).

The lower part of the scheme is the electronic properties, which include the conductivity, plasma frequency, and electronic density of states (DOS). The DOS directly arises from the DFT. The plasma frequency and conductivity are determined by the imaginary part of the DF (5). The values of plasma frequency of shock-compressed xenon plasma are calculated in Ref. [19] with the DF, which also gives good agreement of calculated values of conductivity and normal reflectivity with the experiment. These results can be considered as a validation of the approach.

The electronic properties are calculated within the framework of the approach also for warm dense hydrogen and liquid selenium [22] in the region of densities and temperatures, where the first-order phase transition is observed experimentally. The calculated values of the conductivity, plasma frequency, and DOS demonstrate the dependence on plasma density, which is characteristic for the first-order phase transitions.

The upper part of the scheme describes the optical properties, which include reflectance (both normal and polarized), Brewster angle, absorption, and transmission. Corrections are considered which allow for the finite width of the transient layer at the WDM border. The optical properties are determined by the complex DF (1) with the real part of the DF obtained from (5) by means of the Kramers-Kronig transformation (6).

As it is mentioned above, the imaginary part of the DF is included in the expressions for both the reflectivity and the plasma frequency. The approach of calculation of the plasma frequency and the effective free-electron density based on using the sum rule is suggested in Ref. [19]. One and the same sum over states defines explicitly both values. Therefore, the values of the plasma frequency calculated within the framework of the approach are directly associated with the dependencies of the reflectivity on the plasma density. It allows us to provide an approach for self-consistent description of optical and electronic properties.

The upper part of the scheme is considered in the given work for the shock-compressed xenon plasma. The approach is extended for the description of normal and polarized reflectivity from the broadened optically nonuniform shock-wave front, using the calculation results for the DF obtained in previous work [19]. The results are compared with the experimental data [11–14].

III. NORMAL REFLECTANCE FROM THE NONUNIFORM DENSITY PROFILE

The method of calculation of the normal reflectance from the sharp border of vacuum and considered medium are presented in Refs. [19,20,40,41], where the comparison with the experimental data for shock-compressed xenon plasmas is given as well. The Fresnel formula is used,

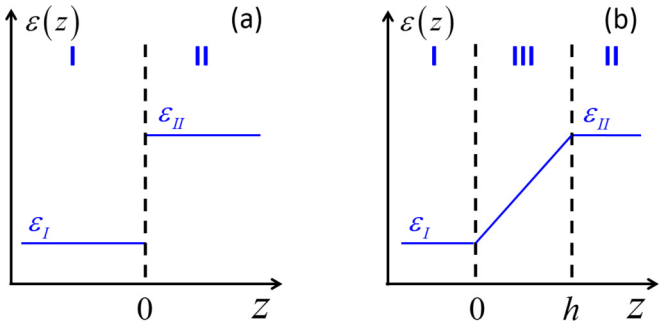

FIG. 2. Schematic dependence of the dielectric function ε on coordinate z on the border of two optically uniform media (I and II), where $z = 0$: (a) the case of the sharp border (dashed line), where the dielectric function changes from $\varepsilon_{\rm I}$ to $\varepsilon_{\rm II}$ abruptly; (b) the border between media I and II is optically nonuniform medium III with the finite width h, where the dielectric function changes continuously.

$$R = \left| \frac{(\sqrt{\varepsilon} - 1)}{(\sqrt{\varepsilon} + 1)} \right|^2. \tag{7}$$

It should be noted that formula (7) is derived for the reflectance of the electromagnetic wave from the sharp border between two optically uniform media with constant values of the DF, as shown in Fig. 2(a). In this case, $\varepsilon_{\rm I} = 1$ (vacuum) and $\varepsilon_{\rm II} = \varepsilon$ and electromagnetic wave comes from region I.

For the general case, the calculation method of the reflectivity [15–18] is based on the solution of the Helmholtz equation,

$$\frac{d^2E(z)}{dz^2} + \frac{4\pi^2}{\lambda^2}\varepsilon(z,\lambda)E(z) = 0, \tag{8}$$

where $E(z)$ is a complex amplitude of the electric field with the wavelength λ, $\varepsilon(z,\lambda)$ is a nonuniform DF of the medium, and z is a coordinate which determines the direction of the electromagnetic wave propagation. The general solution of Eq. (8) in region I ($z < 0$) in Fig. 2 for the DF $\varepsilon(z,\lambda) = \varepsilon_{\rm I} = 1$ is given by the expression

$$E(z) = C_i \exp(2\pi i z/\lambda) + C_r \exp(-2\pi i z/\lambda), \tag{9}$$

where C_i and C_r are the amplitudes of incident and reflected waves, respectively. The values of C_i and C_r can be found from the following set of equations:

$$\begin{aligned} C_i + C_r &= E(0) \\ (2\pi i/\lambda)(C_i - C_r) &= E'(0), \end{aligned} \tag{10}$$

where E' is a derivative dE/dz. The boundary conditions $E(0)$ and $E'(0)$ are determined by the solution of Eq. (8) in the region $z > 0$, which corresponds to region II in Fig. 2(a) or region III in Fig. 2(b).

The reflectivity R is determined by the ratio of the intensities of the reflected and incident waves $|C_r|^2/|C_i|^2$. Substitution of the solution of the set of equations (10) gives the following expression for the reflectivity:

$$R = \frac{|C_r|^2}{|C_i|^2} = \left| \frac{2\pi i E(0) - \lambda E'(0)}{2\pi i E(0) + \lambda E'(0)} \right|^2. \tag{11}$$

For the reflection from the sharp border between two optically uniform media [Fig. 2(a)] with permittivities $\varepsilon_{\rm I} = 1$ and $\varepsilon_{\rm II} = \varepsilon$, the boundary conditions are $E(0) = 1$ and $E'(0) = 2\pi i\sqrt{\varepsilon}/\lambda$, which correspond to the solution of Eq. (8) $E(z) = \exp(2\pi i\sqrt{\varepsilon}z/\lambda)$ in the region $z > 0$. Substitution of these boundary conditions into (11) gives the well-known Fresnel formula (7).

In this work, we consider the reflection of the electromagnetic wave from the spatially broadened border of vacuum and considered medium. In the general case, the border between vacuum and the shock-compressed medium is not steplike. It is characterized by smearing of the density profile within the region with finite width. The region corresponds to the broadened shock-wave front. In this region, the optical parameters, such as DF and refraction, change continuously as schematically shown in Fig. 2(b). Therefore, such a region is optically nonuniform. In this case, the Fresnel formula (7) is inapplicable, since the solution of Eq. (8) in the region III $0 < z < h$ differs from $E(z) = \exp(2\pi i\sqrt{\varepsilon}z/\lambda)$ in the region $z > 0$. In order to find the values $E(0)$ and $E'(0)$, Eq. (8) is to be solved for the range $0 < z < h$ with the following boundary conditions at $z = h$:

$$E(h) = \exp[2\pi i\sqrt{\varepsilon(h,\lambda)}h/\lambda],$$
$$E'(h) = (2\pi i/\lambda)\sqrt{\varepsilon(h,\lambda)}E(h), \qquad (12)$$

where h is the width of the optically nonuniform region. The linear approximation for the dependence of the DF on distance z is applied $\varepsilon(z,\lambda) = 1 + [\varepsilon(h,\lambda) - 1](z/h)$ in region III.

The value of the $\varepsilon(h,\lambda)$ is calculated within the framework of the DFT by formulas (5) and (6). Within the framework of the DFT, the generalized gradient approximation (GGA) for the exchange and correlation part of the density functional is used. The functional of Perdew, Burke, and Ernzerhof (PBE) [44] is used. The solution of the Kohn-Sham equations is found as a superpositions of the plane waves. The energy cutoff of the plane-waves basis set is 180 eV, which provides the convergence of the results.

Calculations are performed in the canonical ensemble. The ion temperature is controlled by the Nosé-Hoover thermostat [45,46]. The electron temperature coincides with the ion temperature and is established by the Fermi-Dirac distribution for occupancies $f(T,E)$. The temperature of the system considered is $T \sim 30\,000$ K. The exact values of temperature corresponding to each value of plasma density are given in Table I. The data in Table I coincide with the experimental values [11–14,18].

TABLE I. Densities ρ and temperatures T [11–14,18].

$\lambda = 1064$ nm		$\lambda = 694$ nm, 532 nm	
ρ (g/cm^3)	T (K)	ρ (g/cm^3)	T (K)
0.51	30 050	0.53	32 900
0.97	29 570	1.1	33 100
1.46	30 260	1.6	33 120
1.98	29 810	2.2	32 090
2.7	29 250	2.8	32 020
3.84	28 810	3.4	31 040

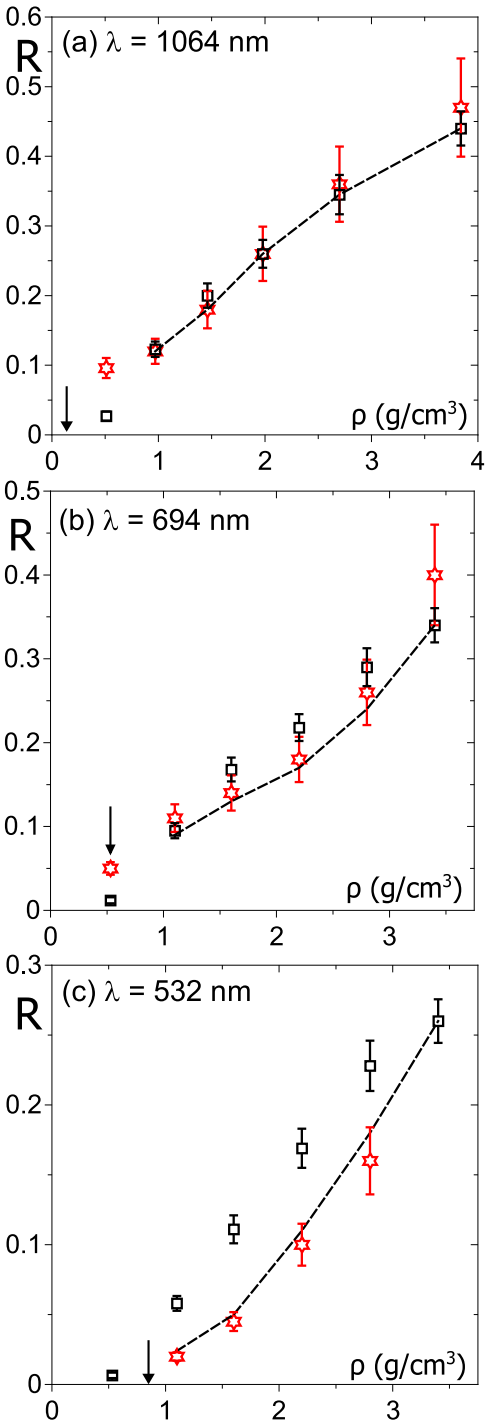

FIG. 3. Dependencies of the shocked xenon plasma reflectivity on the plasma density at various values of wavelengths 1064 nm (a), 694 nm (b), and 532 nm (c). The experimental data [11,12,18] are depicted by stars. The squares correspond to the calculated reflectivities from the sharp wave front. The arrows indicate the values of the plasma density, where the frequency of incident radiation and the plasma frequency coincide with each other. The dashed lines are calculated reflectivities from the broadened wave front.

The measured and calculated dependencies of the reflectivity on density are shown in Fig. 3 for the wavelengths of laser radiation 1064 nm [Fig. 3(a)], 694 nm [Fig. 3(b)],

TABLE II. The width of the wave front h (nm) for various values of the density ρ (g/cm^3) and wavelengths λ.

ρ	0.97	1.46	1.98	2.7	3.84
$\lambda = 1064$ nm	0–130	0–145	0–110	0–80	0–70
ρ	1.1	1.6	2.2	2.8	3.4
$\lambda = 694$ nm	0–135	60–145	40–112	0–110	0–25
$\lambda = 532$ nm	130–180	130–175	96–120	75–115	—

and 532 nm [Fig. 3(c)]. The experimental data [11,12,18] are depicted by stars with the error bars. The squares correspond to the calculation results obtained in Refs. [19,40,41] without introduction of wave-front broadening. As one can see, the calculated reflectivities for the wavelengths 1064 and 694 nm [Fig. 3(a) and 3(b)] are in a good agreement with the experimental data both in the absolute values and in the density dependence. Theoretical values of the reflectivity at 532 nm are overestimated in comparison with the experimental ones. However, the relative dependence of the reflection coefficient on the density is reproduced.

The wave-front width h is a parameter of Eq. (8). It is possible to choose the range of values of h, which gives the exact experimental values of reflectances at each density within the error bars. The values of the width h are given in Table II. The range of h in Table II is determined by the experimental error of measurement of reflectivity.

The dependence of reflectivity on density calculated by formula (11) is depicted by dashed line in Fig. 3. The introduction of wave-front broadening improves the agreement with the experiment for wavelength $\lambda = 532$ nm and, at the same time, it does not make worse the agreement for $\lambda = 694$ nm. Therefore, since the values of the width are close to the theoretical value 100 nm, which is physically justified, the approach gives a complete explanation of the experimental data [12,18].

IV. POLARIZED REFLECTIVITY FROM SHARP SHOCK-WAVE FRONT

If the wave vector of the incoming electromagnetic wave is not collinear with the surface normal, then the reflectivity depends on polarization of the incident wave. In this case, the incident wave should be separated into two polarizations for description of reflectivity. The s-polarized wave is determined by the component of the electric field, which is perpendicular to the plane of incidence. The components of the electric field, which are parallel to the incident plane, correspond to the p polarization. The following Fresnel formulas are used for the calculation of reflectivity of s- and p-polarized waves from the sharp border of vacuum and considered medium:

$$R_s = \left| \frac{\cos\varphi - \sqrt{\varepsilon - \sin^2\varphi}}{\cos\varphi + \sqrt{\varepsilon - \sin^2\varphi}} \right|^2, \tag{13a}$$

$$R_p = \left| \frac{\varepsilon\cos\varphi - \sqrt{\varepsilon - \sin^2\varphi}}{\varepsilon\cos\varphi + \sqrt{\varepsilon - \sin^2\varphi}} \right|^2, \tag{13b}$$

where φ is the incident angle.

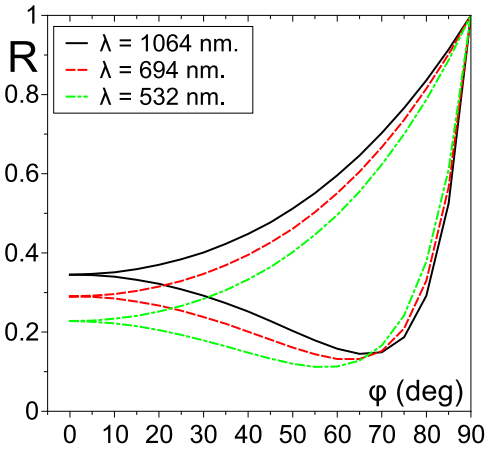

FIG. 4. Calculated dependencies of the shocked xenon plasma s-polarized (upper lines) and p-polarized (lower lines) reflectivities on the incident angle at various values of wavelengths and density: $\lambda = 1064$ nm and $\rho = 2.7$ g/cm^3 (solid lines); $\lambda = 694$ nm and $\rho = 2.8$ g/cm^3 (dashed lines); and $\lambda = 532$ nm and $\rho = 2.8$ g/cm^3 (dash-dotted lines).

The DF is determined by formulas (5) and (6) within the framework of the DFT. It is used for the calculation of the polarized reflectivities by the expressions (13). In Fig. 4, the results of the calculation of reflectivities from xenon plasmas of the s-polarized (upper lines) and p-polarized (lower lines) waves are shown for the three wavelengths $\lambda = 1064$ nm (solid lines), 694 nm (dashed lines), and 532 nm (dash-dotted lines). The incident angle, at which the p-polarized reflectivity reaches the minimum value, is the Brewster angle. The minimum differs from zero due to the considerable conductance and absorbtion of the xenon plasma.

V. POLARIZED REFLECTIVITY FROM BROADENED SHOCK WAVE FRONT

For the calculation of the dependence of the s-polarized electric field $E(z)$ amplitude on incident angle φ, the expression $\varepsilon(z,\lambda) - \sin^2\varphi$ is to be substituted in (8) and in the boundary conditions (12) instead of $\varepsilon(z,\lambda)$. The amplitude of the p-polarized magnetic field $H(z,\varphi)$ is a solution of the equation

$$\varepsilon(z,\lambda)\frac{\partial}{\partial z}\left[\frac{1}{\varepsilon(z,\lambda)}\frac{\partial H(z,\varphi)}{\partial z}\right] + [\varepsilon(z,\lambda) - \sin^2\varphi]H(z,\varphi) = 0, \tag{14}$$

with the corresponding boundary conditions,

$$H(h,\varphi) = \exp[2\pi i\sqrt{\varepsilon(h,\lambda) - \sin^2\varphi}\,h/\lambda],$$
$$H_z(h,\varphi) = (2\pi i/\lambda)\sqrt{\varepsilon(h,\lambda) - \sin^2\varphi}\,H(h,\varphi), \tag{15}$$

where $H_z = \partial H/\partial z$. The p-polarized reflectivity is calculated by the following formula:

$$R_p(\varphi) = \left| \frac{2\pi i\sqrt{1 - \sin^2\varphi}\,H(0,\varphi) - \lambda H_z(0,\varphi)}{2\pi i\sqrt{1 - \sin^2\varphi}\,H(0,\varphi) + \lambda H_z(0,\varphi)} \right|^2. \tag{16}$$

TABLE III. The widths of the wave front. The values of the wave-front widths are obtained as a parameters of the solution of the Helmholtz equations (h_1) and from the Drude theory (h_2)

λ (nm), ρ (g/cm^3)	h_1 (nm)	h_2 (nm)
1064, 2.7	80	161
694, 2.8	100	154
532, 2.8	100	145

The expression (16) is obtained by the same procedure as (11) and coincides with expression 13(b) for the sharp border between the vacuum and considered medium. For the calculation of the s-polarized reflectivity, the corresponding values of the amplitude $E(0,\varphi)$ and its derivative $E_z(0,\varphi)$ are to be substituted into (16) instead of $H(0,\varphi)$ and $H_z(0,\varphi)$.

The estimated values of the widths are presented in Table III. The values (h_1) correspond to the values of the shock-wave width calculated as the solution parameters of the Helmholtz equations (14).

The measured and calculated values of the R_s and R_p reflectivity dependencies on the incident angle φ are shown in Fig. 5 for the wavelengths of laser radiation 1064, 694, and 532 nm and densities 2.7 and 2.8 g/cm^3. The experimental data [13,14] are depicted by squares (R_s) and circles (R_p). The solid lines coincide with the results shown in Fig. 4 obtained without introduction of the broadening of the wave front for each value of the wavelength, respectively. Dashed lines correspond to the results calculated with introduction of the wave-front broadening, with the width h_1.

The depth of the wave front h can be also estimated within the framework of the Drude theory [47–49] for the polarized reflection of the electromagnetic wave using the experimental dependences of R_s and R_p on incident angle φ. For this approach, the magnitude of h can be evaluated from the equation

$$\frac{R_p}{R_s} = \frac{\pi^2 h^2}{\lambda^2}\left|\frac{n^2+1}{(n^2-1)^2}\beta^2\right|, \tag{17}$$

where n is a refraction coefficient of the plasma, $\beta = \overline{N^2} + n^2(\overline{1/N^2}) - 1 - n^2$, and $N = N(z) = \sqrt{\varepsilon(z,\lambda)}$ is the nonuniform refraction coefficient. The upper line averages over the width of the transitive layer (wave front). The ratio R_s/R_p is found at a value of the Brewster angle φ_B, where R_p reaches the minimum value. For the linear dependence of $N(z)$, the expression (17) gives the following result for h:

$$h = \lambda\left[\left(\frac{3}{2\pi}\right)\left(\frac{R_p}{R_s}\right)^{1/2}(R|n^2+1|)^{-1/2}\right], \tag{18}$$

where R is a reflection coefficient for the normal incidence. The refraction coefficient $n = \sqrt{\varepsilon}$ is calculated within the framework of the DFT. The values h_2 in Table III are estimated by formula (18) within the framework of the Drude theory of reflection. As one can see, this method also gives the estimation of the width, which is smaller than the estimations of Refs. [13,14] and closer to the theoretical value 100 nm [11].

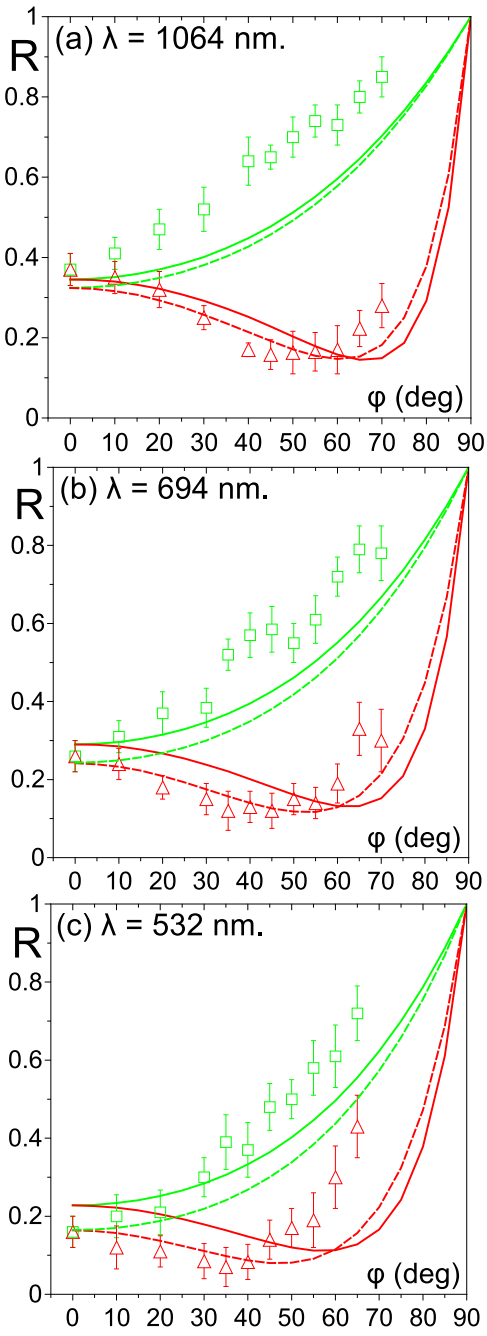

FIG. 5. Dependencies of the shocked xenon plasma R_s (green) and R_p (red) reflectivities on the incident angle at various values of wavelengths and density. The experimental data [13,14] are depicted by squares (R_s) and circles (R_p). The solid lines correspond to the calculation results, which are obtained without introduction of wavefront broadening. The dashed lines correspond to the calculated values of the reflectivity with the broadened wavefront.

VI. BREWSTER ANGLE

The Brewster angle is an angle of incidence at which the reflectivity of the p-polarized component of the electromagnetic wave reaches the minimum value. Experimental and calculated values of the Brewster angles φ_B are given in Table IV. The experimental values of the Brewster angles [13,14] are shown

TABLE IV. Brewster angles.

	φ_B (degrees)		
λ (nm), ρ (g/cm^3)	Refs. [13,14]	Sharp front	Broadened front
1064, 2.7	50 ± 10	70	60
694, 2.8	45 ± 10	65	55
532, 2.8	35 ± 5	55	45

in the second column. The values of φ_B in the third column correspond to the minimum values of the R_p calculated by the Fresnel formula (13) for the sharp wave front ($h = 0$ nm). The values in the fourth column correspond to the minima of p-polarized reflectivity calculated by formula (16) with introduction of the shock-wave front broadening.

One can see that the calculated minima of the dependencies $R_p(\varphi)$ obtained for the case of the sharp front are shifted relatively to the experimental ones. The introduction of wave-front broadening improves the agreement with the experiment. This result can be considered a notification of the existence of the transitive region with finite width, where the refraction changes continuously due to a smooth increase of the plasma density.

VII. CONCLUSIONS

The self-consistent approach for the calculation of the optical and electronic properties of warm dense matter and nonideal plasmas [19–23] is modified to extend its application for the description of reflectance from the broadened shock-wave front and for the incidence of radiation at an arbitrary angle. Expressions (8)–(18) are applied with the DF obtained in Ref. [19].

(1) Within the framework of the approach, the method of the calculation of reflectivity is applied, which is based on the solution of the Helmholtz equation for the amplitudes of the electromagnetic field. The method allows to take into account the nonuniformity of the density profile (shock-wave front broadening) and is used for the calculation of the normal reflectivity as well as for s- and p-polarized reflectivities for a number of incident angles.

(2) Another method is considered, which is based on the Drude theory [47,48] of reflection. It allows us to calculate the ratio of the s- and p-polarized reflectances if the dependence of the dielectric function on distance is known.

(3) The inverse problem is solved: The width of the shock-wave front is estimated based on calculated values of reflectivity and dielectric function. The width values are considered as a parameter of the solution of the Helmholtz equation.

The additional method of the estimation of the width is suggested. It allows us to estimate the wave-front width using the experimental ratio of s- and p-polarized reflectivities within the framework of the Drude theory of refraction from an optically nonuniform medium.

Both values of the wave-front width are closer to the physically approved width of propagation of electron avalanche in shock-compressed xenon contrary to the results [14,17,18].

(4) The reflectivities calculated with taking into account of the shock-wave broadening are in a good agreement with the experimental data for xenon plasmas [11–14].

ACKNOWLEDGMENTS

Authors thank V. B. Mintsev and Yu. B. Zaporozhets for the information about the results of the measurements. The calculations were carried out on the computing clusters MVS-100K of the Joint Supercomputer Center RAS and K-100 of the Keldysh Institute of Applied Mathematitcs RAS. The work is supported by Grant No. 14-19-01295 of the Russian Science Foundation.

[1] M. A. Morales, J. M. McMahon, C. Pierleoni, and D. M. Ceperley, Phys. Rev. Lett. **110**, 065702 (2013).
[2] G. Huser, N. Ozaki, T. Sano, Y. Sakawa, K. Miyanishi, G. Salin, Y. Asaumi, M. Kita, Y. Kondo, K. Nakatsuka, H. Uranishi, T. Yang, N. Yokoyama, D. Galmiche, and R. Kodama, Phys. Plasmas **20**, 122703 (2013).
[3] G. Huser, V. Recoules, N. Ozaki, T. Sano, Y. Sakawa, G. Salin, B. Albertazzi, K. Miyanishi, and R. Kodama, Phys. Rev. E **92**, 063108 (2015).
[4] M. D. Knudson, M. P. Desjarlais, A. Becker, R. W. Lemke, K. R. Cochrane, M. E. Savage, D. E. Bliss, T. R. Mattsson, and R. Redmer, Science **348**, 1455 (2015).
[5] K. Ohta, K. Ichimaru, M. Einaga, S. Kawaguchi, K. Shimizu, T. Matsuoka, N. Hirao, and Y. Ohishi, Sci. Rep. **5**, 16560 (2015).
[6] M. Zaghoo, A. Salamat, and I. F. Silvera, Phys. Rev. B **93**, 155128 (2016).
[7] Y. V. Petrov, N. A. Inogamov, and K. P. Migdal, J. Exp. Theor. Phys. Lett. **97**, 20 (2013).
[8] L. A. Falkovsky, Phys. Rev. B **77**, 193201 (2008).
[9] L. A. Falkovsky, J. Exp. Theor. Phys. **115**, 1151 (2012).
[10] M. E. Veysman and N. E. Andreev, J. Phys.: Conf. Ser. **653**, 012004 (2015).
[11] V. B. Mintsev and Y. B. Zaporozhets, Contrib. Plasma Phys. **29**, 493 (1989).
[12] Y. B. Zaporoghets, V. B. Mintsev, V. K. Gryaznov, and V. E. Fortov, in *Physics of Extreme States of Matter*, edited by V. E. Fortov (Inst. Probl. Chem. Phys. RAN, Chernogolovka, 2002), pp. 188–189, [in Russian].
[13] Y. B. Zaporoghets, V. B. Mintsev, V. K. Gryaznov, V. E. Fortov, H. Reinholz, and G. Röpke, in *Physics of Extreme States of Matter*, edited by V. E. Fortov (Inst. Probl. Chem. Phys. RAN, Chernogolovka, 2009), pp. 194–197.
[14] Y. B. Zaporozhets, V. B. Mintsev, V. K. Gryaznov, H. Reinholz, G. Röpke, Y. A. Omarbakiyeva, and V. E. Fortov, J. Phys.: Conf. Ser. **653**, 012110 (2015).
[15] H. Reinholz, G. Röpke, A. Wierling, V. Mintsev, and V. Gryaznov, Contrib. Plasma Phys. **43**, 3 (2003).
[16] H. Reinholz, G. Röpke, I. Morozov, V. Mintsev, Y. Zaparoghets, V. Fortov, and A. Wierling, J. Phys. A: Math. Gen. **36**, 5991 (2003).

[17] H. Reinholz, Y. Zaporoghets, V. Mintsev, V. Fortov, I. Morozov, and G. Röpke, Phys. Rev. E **68**, 036403 (2003).
[18] Y. Zaporoghets, V. Mintsev, V. Gryaznov, V. Fortov, H. Reinholz, T. Raitza, and G. Röpke, J. Phys. A: Math. Gen. **39**, 4329 (2006).
[19] G. Norman, I. Saitov, V. Stegailov, and P. Zhilyaev, Phys. Rev. E **91**, 023105 (2015).
[20] G. E. Norman, I. M. Saitov, and V. V. Stegailov, J. Exp. Theor. Phys. **120**, 894 (2015).
[21] G. E. Norman and I. M. Saitov, J. Phys.: Conf. Ser. **653**, 012111 (2015).
[22] G. E. Norman, I. M. Saitov, and V. V. Stegailov, Contrib. Plasma Phys. **55**, 215 (2015).
[23] I. M. Saitov, Mol. Phys. **114**, 446 (2016).
[24] A. F. Starace, Phys. Rev. A **3**, 1242 (1971).
[25] R. Kubo, J. Phys. Soc. Jpn. **12**, 570 (1957).
[26] D. A. Greenwood, Proc. Phys. Soc. **71**, 585 (1958).
[27] V. Recoules, P. Renaudin, J. Clérouin, P. Noiret, and G. Zérah, Phys. Rev. E **66**, 056412 (2002).
[28] V. Recoules and J.-P. Crocombette, Phys. Rev. B **72**, 104202 (2005).
[29] V. Recoules, F. Lambert, A. Decoster, B. Canaud, and J. Clérouin, Phys. Rev. Lett. **102**, 075002 (2009).
[30] D. V. Knyazev and P. R. Levashov, Phys. Plasmas **21**, 073302 (2014).
[31] R. Del Sole and R. Girlanda, Phys. Rev. B **48**, 11789 (1993).
[32] H. Ehrenreich and M. H. Cohen, Phys. Rev. **115**, 786 (1959).
[33] S. L. Adler, Phys. Rev. **126**, 413 (1962).
[34] N. Wiser, Phys. Rev. **129**, 62 (1963).
[35] G. Kresse and J. Hafner, Phys. Rev. B **47**, 558 (1993).
[36] G. Kresse and J. Hafner, Phys. Rev. B **49**, 14251 (1994).
[37] G. Kresse and J. Furthmüller, Phys. Rev. B **54**, 11169 (1996).
[38] G. Kresse and D. Joubert, Phys. Rev. B **59**, 1758 (1999).
[39] M. Gajdoš, K. Hummer, G. Kresse, J. Furthmüller, and F. Bechstedt, Phys. Rev. B **73**, 045112 (2006).
[40] G. Norman, I. Saitov, V. Stegailov, and P. Zhilyaev, Contrib. Plasma Phys. **53**, 300 (2013).
[41] G. Norman, I. Saitov, V. Stegailov, and P. Zhilyaev, Contrib. Plasma Phys. **53**, 503 (2013).
[42] I. V. Morozov and G. E. Norman, J. Exp. Theor. Phys. **100**, 370 (2005).
[43] H. B. Nersisyan, M. E. Veysman, N. E. Andreev, and H. H. Matevosyan, Phys. Rev. E **89**, 033102 (2014).
[44] J. P. Perdew, A. Ruzsinszky, G. I. Csonka, O. A. Vydrov, G. E. Scuseria, L. A. Constantin, X. Zhou, and K. Burke, Phys. Rev. Lett. **100**, 136406 (2008).
[45] S. Nosé, J. Chem. Phys. **81**, 511 (1984).
[46] W. G. Hoover, Phys. Rev. A **31**, 1695 (1985).
[47] P. Drude, Ann. Phys. **306**, 566 (1900).
[48] P. Drude, Ann. Phys. **308**, 369 (1900).
[49] O. N. Gadomskiĭ and S. V. Sukhov, Opt. Spectrosc. **89**, 261 (2000).